# **OPEN ACCESS**



# Evidence of a Nonorthogonal X-line in Guide-field Magnetic Reconnection

Neha Pathak 1 , R. E. Ergun , Y. Qi , S. J. Schwartz , T. Vo , M. E. Usanova , M. Hesse , T. D. Phan , J. F. Drake , S. Eriksson , N. Ahmadi , A. Chasapis , F. D. Wilder , J. E. Stawarz , J. L. Burch , K. J. Genestreti , R. B. Torbert , and R. Nakamura , Laboratory for Atmospheric and Space Physics, University of Colorado, Boulder, CO 80303, USA; Neha.Pathak@lasp.colorado.edu 

1 Laboratory for Atmospheric and Planetary Sciences, University of Colorado, Boulder, CO 80303, USA 

3 Imperial College London, London, UK 

4 NASA Ames Research Center, Moffett Field, CA 94035, USA 

5 Space Sciences Laboratory, University of California, Berkeley, CA 94720, USA 

6 University of Maryland, College Park, MD 20742, USA 

7 Department of Physics, University of Texas at Arlington, Arlington, TX 76019, USA 

8 The Blackett Laboratory, Imperial College London, London SW7 2AZ, UK 

9 Southwest Research Institute, San Antonio, TX 78238, USA 

10 University of New Hampshire, Durham, NH 03824, USA 

11 Space Research Institute, Austrian Academy of Sciences, Graz, Austria 
Received 2022 August 16; revised 2022 November 22; accepted 2022 November 26; published 2022 December 22

### **Abstract**

We present observations that suggest the X-line of guide-field magnetic reconnection is not necessarily orthogonal to the plane in which magnetic reconnection is occurring. The plane of magnetic reconnection is often referred to as the L-N plane, where L is the direction of the reversing and reconnecting magnetic field and N is normal to the current sheet. The X-line is often assumed to be orthogonal to the L-N plane (defined as the M-direction) in the majority of theoretical studies and numerical simulations. The four-satellite Magnetospheric Multiscale (MMS) mission, however, observes a guide-field magnetic reconnection event in Earth's magnetotail in which the X-line may be oblique to the L-N plane. This finding is somewhat opportune as two of the MMS satellites at the same N location report nearly identical observations with no significant time delays in the electron diffusion region (EDR) even though they have substantial separation in L. A minimum directional derivative analysis suggests that the X-line is between  $40^\circ$  and  $60^\circ$  from M, adding support that the X-line is oblique. Furthermore, the measured ion velocity is inconsistent with the apparent motion of the MMS spacecraft in the L-direction through the EDR, which can be resolved if one assumes a shear in the L-N plane and motion in the M-direction. A nonorthogonal X-line, if somewhat common, would call for revisiting theory and simulations of guide-field magnetic reconnection, reexamination of how the reconnection electric field is supported in the EDR, and reconsidering the large-scale geometry of the X-line.

*Unified Astronomy Thesaurus concepts:* Space plasmas (1544); Planetary magnetospheres (997); Plasma astrophysics (1261); Plasma physics (2089)

# 1. Introduction

Magnetic reconnection is one of the most impactful phenomena in space (Øieroset et al. 2001; Mozer et al. 2002; Paschmann 2008; Paschmann et al. 2013; Burch et al. 2016; Torbert et al. 2018), laboratory (Yamada et al. 2010), and astrophysical plasmas (Uzdensky 2011; Zweibel Yamada 2009; Lazarian et al. 2015). It comes into play when a magnetic field (B) experiences topological rearrangement (Petschek 1964; Forbes & Priest 1987). One of the most fascinating aspects of magnetic reconnection is that, even though it occurs inside a small diffusion region (Burch & Drake 2009; Hesse et al. 2011), the related changes in the magnetic field can substantially affect the evolution and dynamics of a large-scale system. This phenomenon is invoked to explain electron and ion heating, particle acceleration, turbulence, and energy conversion and transport (Drake et al. 2003; Sundkvist et al. 2007; Eastwood et al. 2009; Roytershteyn et al. 2012; Karimabadi et al. 2013; Phan et al. 2018;

Original content from this work may be used under the terms of the Creative Commons Attribution 4.0 licence. Any further distribution of this work must maintain attribution to the author(s) and the title of the work, journal citation and DOI.

Ergun et al. 2020a). Understanding the 3D behavior of magnetic reconnection on the large scale (e.g., Priest & Schrijver 1999) and in the electron diffusion region (EDR) is a current challenge. Even though patchy reconnection (Paschmann et al. 2013) and deflections of the X-line (Hesse et al. 2013; Genestreti et al. 2018, 2022) are reported, the basic theoretical premise of quasi-2D magnetic reconnection has been that the X-line is orthogonal to the L-N plane, where L is the direction of the reversing and reconnecting B and N is normal to the current sheet. In this Letter, we explore the possibility that the X-line is not orthogonal to the L-N plane in a guide-field magnetic reconnection event. We show that a fortuitous alignment of two of the Magnetospheric Multiscale (MMS) spacecraft and a directional derivative analysis suggest that the X-line, which we call the M'-direction, may lie between  $40^{\circ}$  and  $60^{\circ}$  from normal to the *L-N* plane. A nonorthogonal X-line shears the L-N planes in the M-direction allowing for plasma parameters to vary in M, which differs from a quasistatic, quasi-2D model. This possibility suggests that the electron physics of the EDR may have to be revisited for some cases of guide-field magnetic reconnection or that a fully 3D analysis may be necessary.

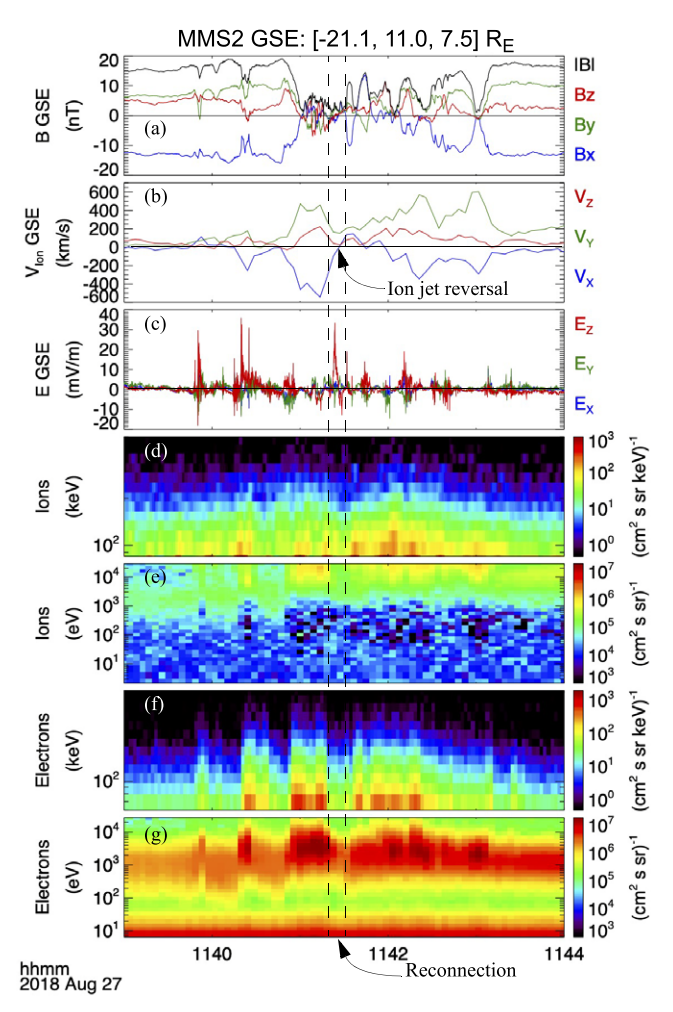


**Figure 1.** Overview of a magnetotail reconnection event on 2018 August 27. From top to bottom: (a)  $\bf B$  in GSE coordinates, (b)  $\bf V_{\rm Ion}$ , (c)  $\bf E$ , (d) omnidirectional ion flux from 70 to 600 keV, (e) differential ion energy flux from 3 eV to 25 keV, (f) omnidirectional electron flux from 60 to 500 keV, and (g) differential electron energy flux from 6 eV to 25 keV.

# 2. Event Overview

We employ data from the four-satellite MMS mission (Burch et al. 2015). The instruments used in this study are the Fluxgate Magnetometer (FGM; Russell et al. 2016), the Electric Field Double Probe (EDP; Ergun et al. 2016; Lindqvist et al. 2016; Torbert et al. 2016), and the Fast Plasma Investigation (FPI; Pollock et al. 2016).

Figure 1 introduces and overviews a magnetic reconnection event on 2018 August 27. The horizontal axis covers 5 minutes, and the vertical dashed lines mark the magnetic reconnection event. The MMS2 satellite was located at [-21.1, 11.0, 7.5] R<sub>E</sub> in the geocentric solar ecliptic (GSE) coordinates in which X is toward the Sun, Z is normal to the solar ecliptic, and Y completes the system. This event has been examined in a recent publication (Li et al. 2021), which concentrates on the generation of Langmuir and upper hybrid waves near the EDR, so our description is brief.

Figure 1(a) displays  $\boldsymbol{B}$  in GSE coordinates, Figure 1(b) the ion velocity ( $V_{\rm Ion}$ ), and Figure 1(c) electric field ( $\boldsymbol{E}$ ). The colors of the traces designate their direction as marked on the right of each panel. Shortly after  $\sim$ 11:40 UT, a strong (>500 km s<sup>-1</sup>), antiearthward ion flow develops (Figure 1(b), blue trace). At  $\sim$ 11:41:26 UT,  $|\boldsymbol{B}|$  decreases and the X-component of  $V_{\rm Ion}$ 

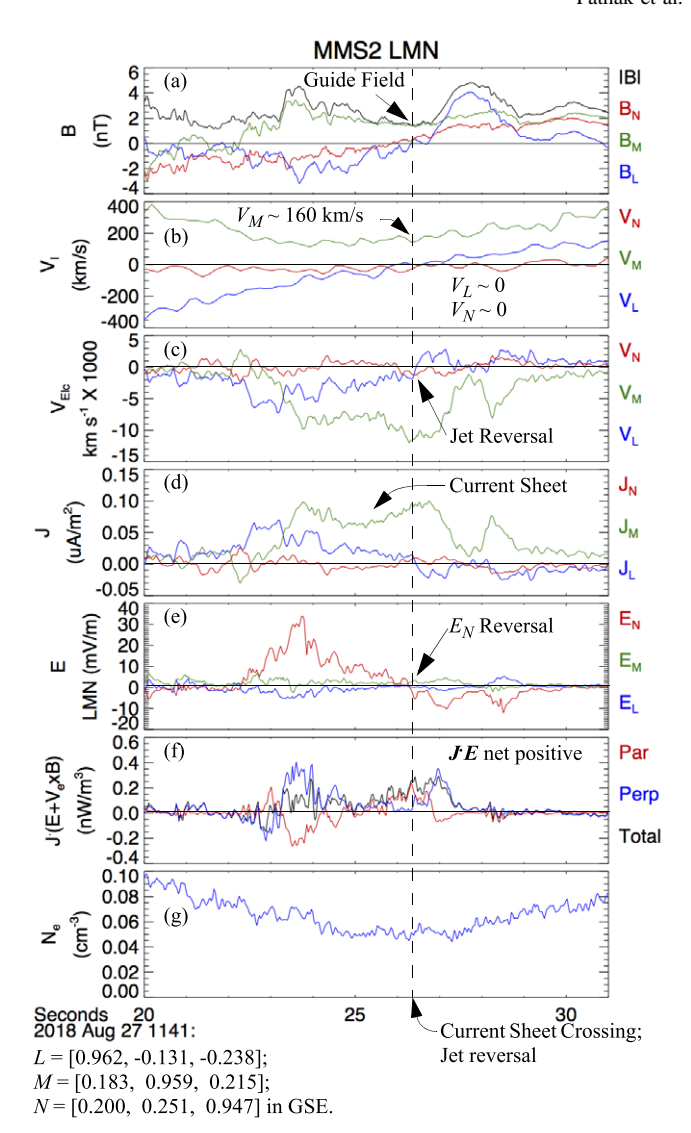


**Figure 2.** A zoomed-in view of the magnetic reconnection event. (a)  $\textbf{\textit{B}}$  in LMN coordinates (written below the figure). (b)  $V_{\text{Ion}}$ . (c)  $V_{\text{Elc}}$ . (d)  $\textbf{\textit{J}}$  derived from electron and ion distributions. (e)  $\textbf{\textit{E}}$ . (f) Electromagnetic energy transfer. (g) The electron density derived from the electron distribution.

reverses, which is a classic signature of an ion jet of magnetic reconnection in Earth's magnetotail (e.g., Li et al. 2021; Torbert et al. 2018). It is noticeable that the ion jet does not remain reversed. After reaching a positive earthward velocity of  $\sim$ 200 km s<sup>-1</sup>, it reverts to being negative, which opens the possibility that the observed event is a secondary X-line after island formation as depicted in several simulations (e.g., Huang & Bhattacharjee 2016; Lapenta et al. 2006). Figure 1(c) shows a large bipolar variation in  $E_z$  (Figure 1(c), red trace) at  $\sim$ 11:41:26 UT, which is the same time that  $V_{\rm Ion}$  reverses. This appears to be a Hall E as the ion motion is not influenced. Figures 1(d)–(g) show accelerated ions and electrons before and after the event. Albeit fairly short in duration, E, E, electron fluxes, and ion fluxes are similar to other turbulent magnetic reconnection events (Ergun et al. 2020a, 2020b).

Figure 2 shows an 11 s zoomed-in view. The data are presented in an LMN coordinate system (e.g., Denton et al. 2018) provided below the plot. The LMN determination, which is critical to this article, is detailed later. In this section, we

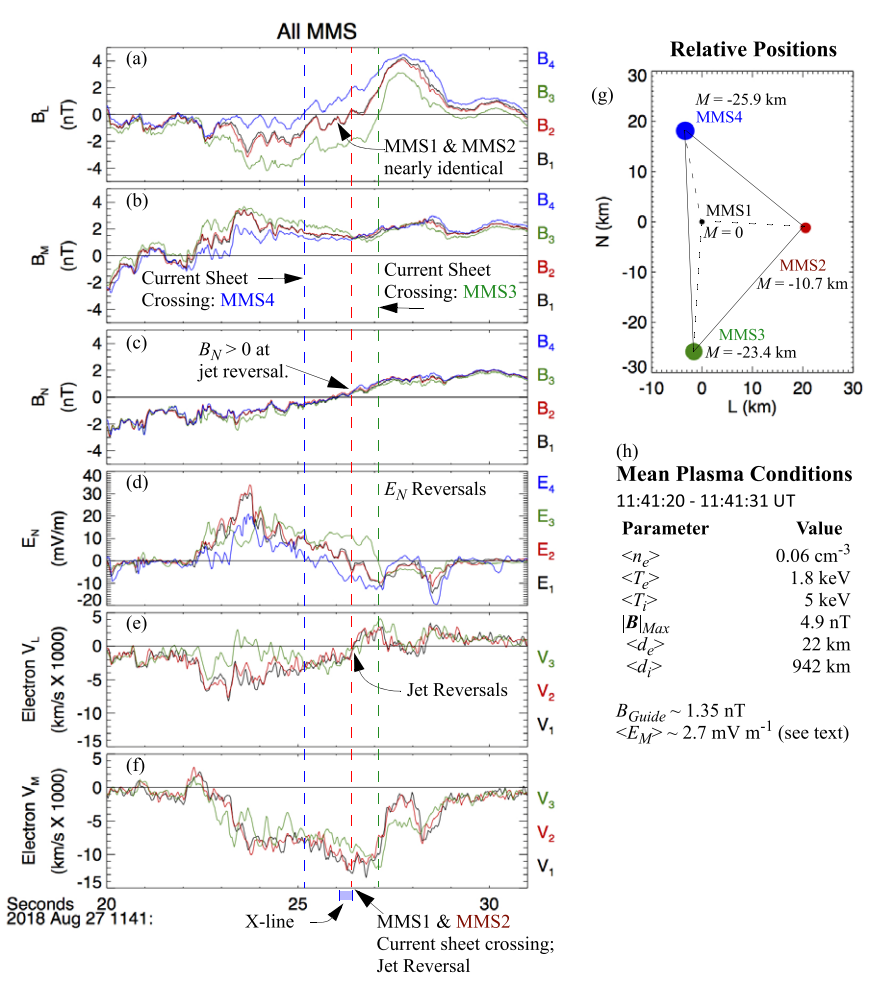


Figure 3. (a)—(c)  $B_L$ ,  $B_M$ , and  $B_N$  from all of the MMS spacecraft. (d) The Hall electric field  $(E_N)$  for each spacecraft. (e)—(f) The electron jet  $V_L$  and the electron current  $V_M$ . The electron jet reversal for MMS1 and MMS2 is at the same time as the current sheet crossing. (g) The relative positions of all the MMS spacecraft. (h) Relevant plasma parameters.

establish that the MMS spacecraft traversed the EDR of guidefield magnetic reconnection.

In the period of Figure 2,  $V_{\rm Ion}$  reverses from tailward to earthward in L (Figure 2(b), blue trace) and, at the same time,  $B_L$  changes from negative to positive (Figure 2(a), blue trace). A strong negative M-directed electron flow ( $V_{\rm Elc}$ ; Figure 2(c), green trace) and the accompanying M current (J; Figure 2(d), green trace) indicate a thin electron current sheet. The netpositive  $\boldsymbol{J} \cdot (\boldsymbol{E} + \boldsymbol{V}_e \times \boldsymbol{B})$  supports that MMS2 is in or near the EDR (Figure 2(f), black line). The  $B_L$  reversal at  $\sim$ 11:41:26.4 UT (Figure 2(a), blue trace) is nearly concurrent with the electron jet reversal (Figures 2(c) and (d), blue traces) and the  $E_N$  reversal (Figure 2(c), red trace), indicating that MMS2 is at or very near to the X-line.  $B_M$  (Figure 2(a), green trace) is  $\sim$ 1.35 nT during the current sheet crossing signifying a guide field.  $E_M$  averages 2.7 mV m<sup>-1</sup> in a 3 s interval surrounding the current sheet crossing (using all spacecraft). The electron density ( $N_e$ ; Figure 2(g)) is  $\sim 0.06$  cm<sup>-3</sup> yielding the electron skin depth  $(d_e)$  of  $\sim 22$  km.

Figures 3(a)–(f) display, in order,  $B_L$ ,  $B_M$ ,  $B_N$ ,  $E_N$ , electron  $V_L$ , and electron  $V_M$  from multiple spacecraft. The colors of the traces designate the spacecraft as indicated on the right of each panel. The MMS tetrahedral formation is shown in Figure 3(g), and relevant plasma parameters are shown in Figure 3(h). The current sheet crossings,  $B_L$  reversals (Figure 3(a)), and  $E_N$  reversals (Figure 3(d)) are marked with vertical dashed lines for

each spacecraft. MMS4 is located at the +N position of the formation and crosses the current sheet first. MMS1 and MMS2 cross the current sheet almost simultaneously, and MMS3, at the -N position of the formation, crosses last. The electron jet  $(V_L)$  reversals of MMS1 and MMS2 (Figure 3(e)) coincide with their current sheet crossings. These data imply that the motion of the MMS spacecraft relative to X-line is in the +N and +L directions (also see Li et al. 2021). Interestingly,  $B_N$  is slightly positive (Figure 3(c)) at the electron jet reversal, which makes the precise location of the X-line ambiguous and may indicate a small asymmetry in this event (Laitinen et al. 2005; Murphy et al. 2010). Figure 3(f) displays the electron  $V_M$  that supports the electron current sheet. High-resolution electron data are not available from MMS4.

Importantly, MMS1 and MMS2 (black and red traces) show almost identical measurements of all parameters even though the two spacecraft are well separated in L (20.5 km). The separation in M is 10.7 km. There is almost no appreciable time delay in any of the measurements between these two spacecraft, which is rather unusual and calls for a deeper investigation.

# 3. Evidence for a Nonorthogonal X-line

The near-identical measurements by MMS1 and MMS2 offer an interesting puzzle as they suggest that the X-line

should lie in the MMS1-MMS2 direction, which is not along M. Furthermore, E and B have a significant, nonzero directional derivative in M (shown later). These observations call into question the quasi-2D picture of magnetic reconnection in which all parameters remain constant along an X-line in the M-direction. Another conundrum comes from the L-component of  $V_{\rm Ion}$ , which is near zero (Figure 2(b)) even though the observations (e.g., electron jet reversals; Figure 3(e)) point to rapid progress in L. In other examples of magnetotail magnetic reconnection (e.g., Torbert et al. 2018), the X-line is found to be embedded in the ion frame in the N-L plane.

These two puzzling aspects in the observations prompted a careful examination of the LMN system. As often done, the Ldirection is estimated as the maximum variance direction of B(Denton et al. 2018). Using the time interval from 11:41:23 to 11:41:28 UT, the maximum variance directions from all spacecraft are within 5° of each other and the eigenvalues are, on average, ~40 times those of the other directions indicating a robust determination of L. However, the two remaining eigenvalues are not well separated, so the Ndirection is estimated from the maximum variance of E, which gives a robust value for N from all four spacecraft. L and N are not normal (10° off), so L is adjusted to be orthogonal to N (justified later with directional derivative analysis). M is set to  $N \times L$ . L obtained in our analysis is within 5° of that reported by Li et al. (2021), and the M-directions are nearly coaligned. A variance analysis using differing time periods and methods (Denton et al. 2018; Genestreti et al. 2022) indicates an uncertainty up to 10°.

An alternative method to determine the M- and N-directions uses a directional derivative analysis (Shi et al. 2019). However, instead of solving the eigenvalue problem point by point and then attempting an average of the of time series data, we opt for a more robust, albeit brute-force, numerical approach. The directional derivative for any scalar  $(\phi)$  is defined as  $n \cdot \nabla \phi$ , where n is a given direction. The directional derivatives of each of the components of B are determined using standard four-spacecraft methods (Dunlop et al. 1988). An average directional derivative for a given n is determined by calculating  $|n \cdot \nabla B|$  then averaging over the time series:

$$DD(\mathbf{n}) = \langle |\mathbf{n} \cdot \nabla \mathbf{B}| \rangle_t. \tag{1}$$

The brute-force approach employs a  $90 \times 360$  array of n vectors to cover a hemisphere in the GSE-Y direction. Figure 4(a) displays the results using GSE  $\mathbf{B}$  that is low-pass filtered (<0.5 Hz) to reduce influence from fluctuations. The directional derivative map (white contours surround the maximum and minimum) shows a maximum within a few degrees of the variance-determined N-direction. However, the minimum directional derivative (M') is nearly  $60^{\circ}$  from the variance-determined M-direction. If one uses M' for M, however, the resulting L' leads to an inconsistent picture of reconnecting magnetic fields ( $B_{M'}$  reverses). Not surprisingly, M' is within  $6^{\circ}$  of the MMS1–MMS2 direction.

The directional derivative analysis is repeated isolating  $B_M(<0.5 \text{ Hz})$ , which has a large signal (Figure 3(b)) that is expected vary in L and N, but not in M. As seen in Figure 4(c), M' is 41° from M. The minimum directional derivative ( $DD_{\text{Min}}$ ) is 3.2 times less than that in the L'-direction ( $DD_{\text{Mid}}$ ), indicating a good determination. The directional derivative of  $E_N$  (<0.5 Hz) results in a 49° angle between M' and M in Figure 4(d) with  $DD_{\text{Mid}}/DD_{\text{Min}} = 5.4$ . The above analysis suggests that the

X-line could be nonorthogonal to the L–N plane as depicted in Figure 4(b).

To investigate the hypothesis of a nonorthogonal X-line further, we map plausible paths of the MMS spacecraft through the EDR. To construct paths, we determine the *N*-position of MMS1 by using

$$J_M = \frac{\partial B_L}{\partial N} - \frac{\partial B_N}{\partial L}.$$
 (2)

Figures 3(a) and (c) indicate that the  $\partial B_L/\partial N$  term dominates. Because the slope of  $B_N$  is nearly constant (Figure 3(c)), the quantity  $\partial B_N/\partial L$  can be treated as a constant, small correction. The *N*-position is then estimated by

$$\Delta N = \frac{\Delta B_L}{J_M + \langle \partial B_N / \partial L \rangle}.$$
 (3)

We set MMS1 at N=0 as it crosses the current sheet and numerically integrate Equation (3) to determine its N-position at any given time. Other spacecraft positions relative to MMS1 are known.

The positions in L are more difficult to determine. The Lcomponent of  $V_{\text{Ion}}$  is near zero at the X-line (Figure 2(b), blue trace), so no physical motion in L between MMS and the X-line is expected. Li et al. (2021) predict a 350 km s<sup>-1</sup> constant speed in L using time delays in  $B_N$ , which we cannot support due to uncertainties in  $B_N$ . The  $\pm 0.05$  nT uncertainty (Russell et al. 2016) makes a  $B_N$ -based velocity determination highly uncertain. Our approach sets the physical motion in L to zero but allows for motion in the M-direction. Motion in the Mdirection can cause the apparent motion in L if L–N planes are sheared (Figure 4(b)). The apparent relative (MMS to X-line) motion in the L-direction is estimated to be 250 km s $^{-1}$  by inspection of several measured quantities (e. g.,  $J_L$  reversal,  $J_M$ peak intensity, and  $V_{\rm Ion}$  reversal). The  $V_{\rm Ion}$  reversal occurs in  $\sim$ 30 s over what is expected to be several ion skin depths (7000-8000 km). The L-speed has an uncertainty of a factor of 2 but, as we show later, it is not critical to our conclusions.

Assuming a shear or nonorthogonal X-line of  $60^{\circ}$ , the MMS spacecraft must be moving  $144 \text{ km s}^{-1}$  in the *M*-direction to realize an apparent motion of  $\sim 250 \text{ km s}^{-1}$  in the *L*-direction (see Figure 4(b)). Because the *M*-component of  $V_{\text{Ion}}$  is positive (Figure 2(b), green trace), the relative speed between the ions and the X-line in the *M*-direction is the sum of  $V_{\text{Ion}}$  and the spacecraft motion, which is  $\sim 300 \text{ km s}^{-1}$ . This relative speed is not unexpected because  $E_M$  accelerates ions in the *M*-direction.

Figures 5(a)-(d) plot  $B_L$ ,  $J_M$ ,  $J_L$ , and  $E_N$  as a function of position using the nonorthogonal X-line model ( $60^{\circ}$  between M and M' and 144 km s<sup>-1</sup> motion along M). Motion in N is physical. In each of the panels, the vertical axis is N, the horizontal axis is the local position in L, and the colors represent the measured values of  $B_L$ ,  $J_M$ ,  $J_L$ , and  $E_N$ .  $J_M$  and  $J_L$ from MMS4 are not available. Because MMS1 and MMS2 overlap, MMS1 is offset by 2 km in N and MMS2 is offset by -2 km in N. The MMS1 and MMS2 traces are half the width of the other traces. The important aspect of this figure is the remarkable agreement between MMS1 and MMS2 and the noteworthy consistency between all of the MMS spacecraft for each of the plotted values.  $B_L$  is negative at negative N, zero when N = 0, and positive at positive N.  $J_M$  peaks in the EDR region.  $J_L$  reverses near-simultaneously at L = 0, and  $E_N$  is also consistent.

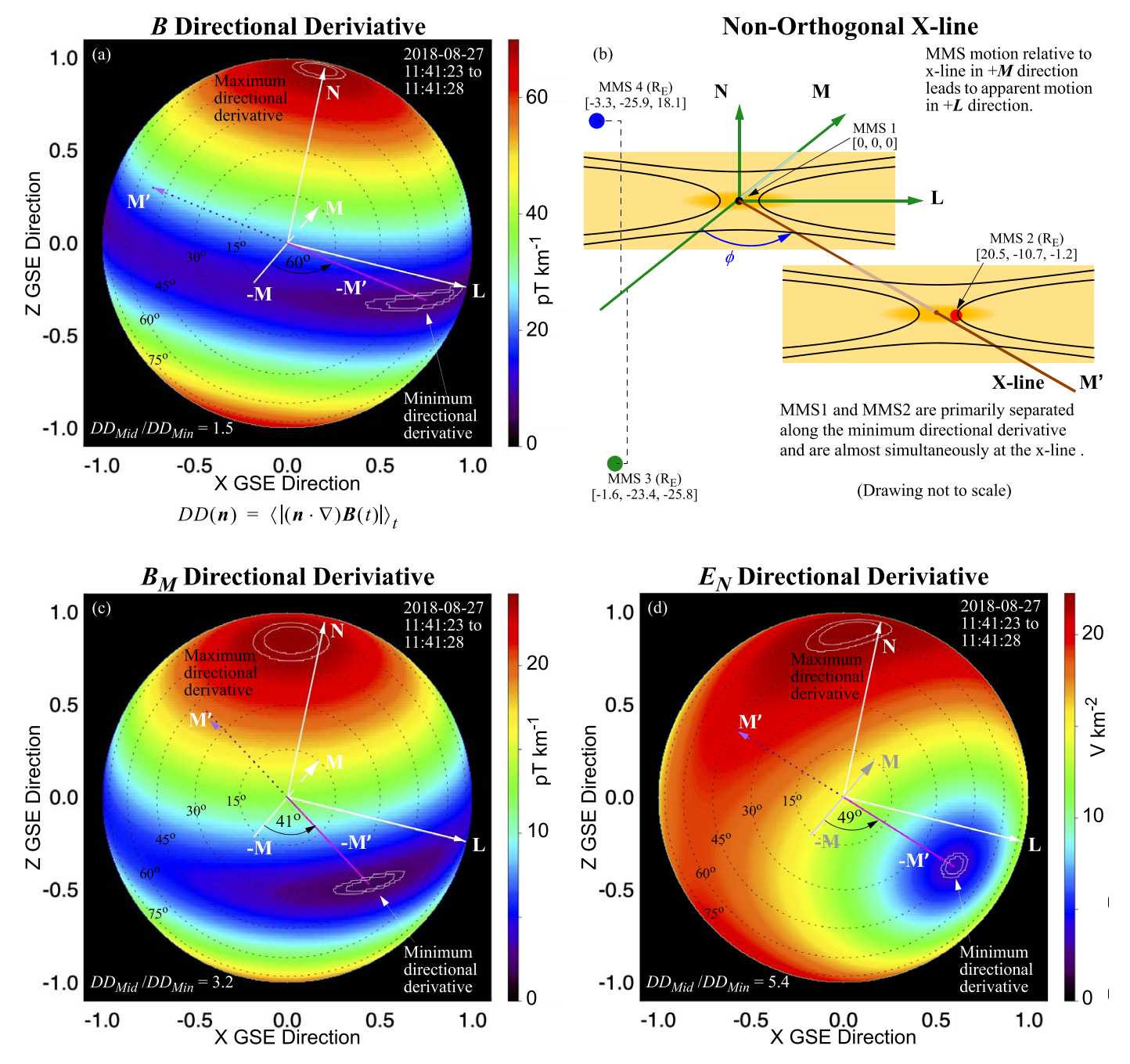


**Figure 4.** (a) The directional derivatives of B in a hemisphere looking from GSE-Y. White contours highlight the minimum and maximum directional derivative is within few degrees of variance-determined N. The minimum directional derivative (M') is  $60^{\circ}$  from variance-determined M and is nearly along the MMS1–MMS2 direction. (b) A cartoon showing that a nonorthogonal X-line sets MMS1 and MMS2 simultaneously at the X-line in the EDR. Because of the shear in the L-N planes, motion in the M-direction leads to apparent motion in the L-direction. The directional derivatives of (c)  $B_M$  and (d)  $E_N$ .

It is most important to realize that the noteworthy consistency and agreement would not necessarily materialize if one uses physical motion in L because MMS1 and MMS2 are separated in L. Figure 5(e) shows a magnified view of  $J_L$  from the nonorthogonal model in which the  $J_L$  reversals of MMS1 and MMS2 are aligned. The MMS3  $J_L$  reversal is also aligned, with lower certainty. Figure 5(f) shows the paths using physical motion in L. The  $J_L$  reversals of MMS1 and MMS2 are misaligned.

# 4. Discussion and Conclusions

A guide-field magnetic reconnection event is observed by MMS as depicted in Figures 2, 3, and 5, and as suggested in a separate study (Li et al. 2021). As the MMS spacecraft transit the EDR, the signatures of  $B_L$ ,  $B_M$ ,  $B_N$ ,  $E_N$ ,  $J_L$ , and  $J_M$  appear to conform very closely to the expected behavior in magnetic reconnection. There are, however, some puzzling features. The most noticeable and somewhat fortuitous feature is that MMS1 and MMS2 observations are nearly identical and exhibit no significant time delay even though the two spacecraft are well separated in L. A minimum directional derivative analysis supports a  $\sim$ 40° to  $\sim$ 60° angle between M' and M, which is

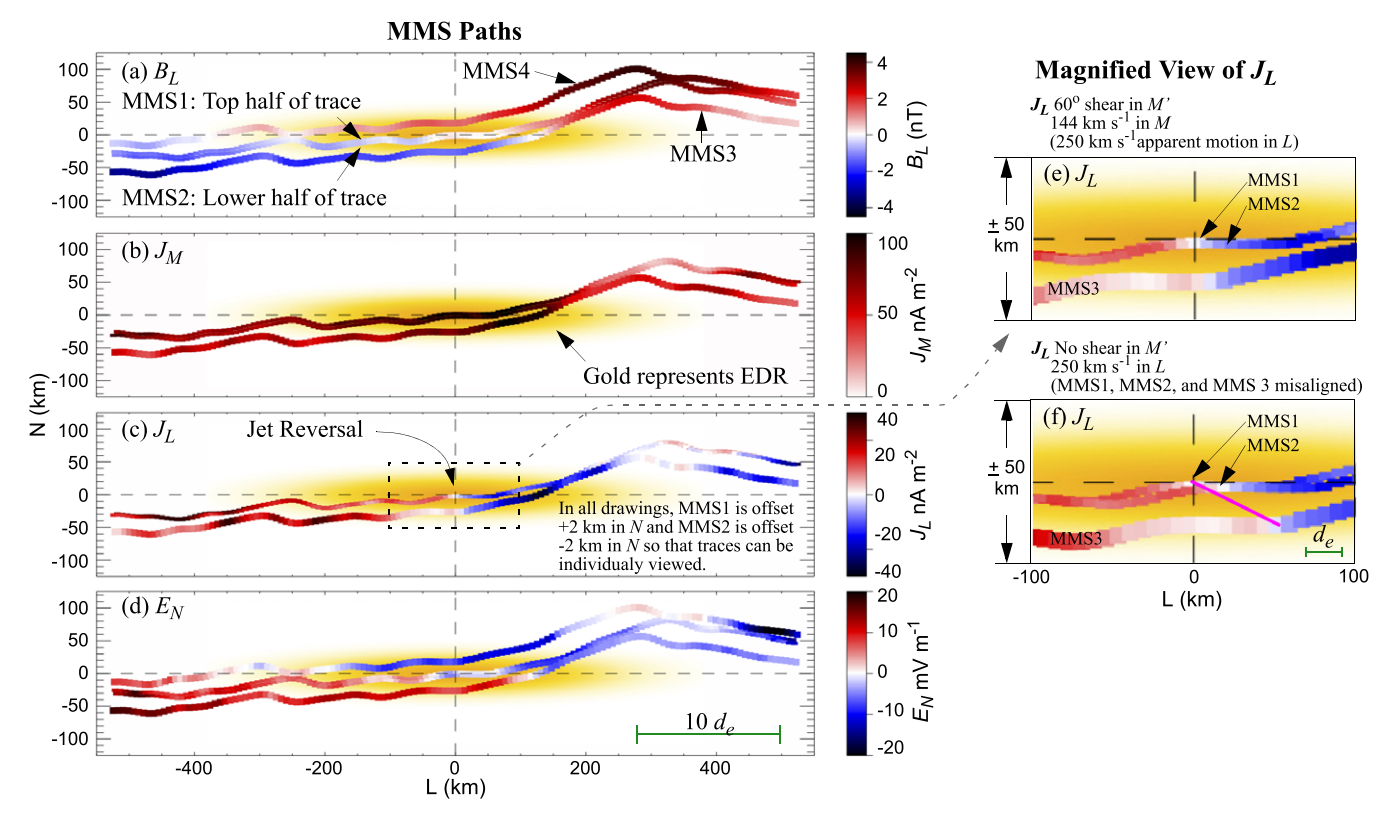


Figure 5. ((a)–(d)) Measured values of  $B_L$ ,  $J_M$ ,  $J_L$ , and  $E_N$  along their estimated paths through the EDR using the nonorthogonal model. The gold area represents the EDR. The MMS1 path is offset 2 km in N, and the MMS2 path is offset -2 km in N so that both can be seen. The MMS1 and MMS2 traces are half the width of the other traces. (e) A zoomed-in view of  $J_L$  along the MMS paths. MMS1, MMS2, and MMS3 show the jet reversal at nearly the same position under the nonorthogonal model. (f) The jet reversal is misaligned using a model with physical motion in L.

well beyond the uncertainties in LMN or M'.  $V_{\text{Ion}}$  reverses but is nearly zero in the EDR whereas the spacecraft appear to rapidly progress in the L-direction.

We interpret these discrepancies as evidence of a non-orthogonal X-line. This interpretation explains the discrepancies, but we have certainly not exhausted all other possibilities. A local disturbance is unlikely because the features that suggest a nonorthogonal X-line do not appear only in the EDR. The near-exact agreement between MMS1 and MMS2 endures for roughly 10 s, during which the spacecraft visited >1000 km of the X-line, which is up to several ion skin depths. This particular event may have been transient in that the ion jets appeared to endure for only several minutes (Figure 1); it is not known whether the transient nature of the event is related to the possible nonorthogonal X-line.

The cause of a nonorthogonal X-line is not clear. There is no strong theoretical argument prohibiting such a feature that the authors are aware of. Large-scale forcing is one possibility. For example, island formation is feasible for this event and may force the X-line geometry. Small-scale processes also may play a role. Interestingly, the X-line in this event is nearly parallel to  $\boldsymbol{B}$  immediately outside of the electron current sheet on the -N side, which may suggest asymmetry. The M-direction of asymmetric guide-field reconnection has been shown to be ambiguously determined (Hesse et al. 2013; Liu et al. 2018).

Several other magnetic reconnection events have also been tested by comparing the minimum directional derivative to the variance-determined M (not always feasible). A near antiparallel event in the magnetotail with otherwise similar plasma conditions (Torbert et al. 2018) is consistent with an orthogonal X-line. A moderate guide-field event in the magnetosheath with

quite different plasma conditions (Wilder et al. 2016) displays a possible  $20^{\circ}$  to  $30^{\circ}$  nonorthogonal X-line. Further studies are needed to determine if a nonorthogonal X-line is common or rare.

The possibility of a nonorthogonal X-line may call for a reexamination of how  $E_M$  is supported in the EDR of guidefield magnetic reconnection. For example, because the L-N planes are sheared, a direct, quasistatic pressure gradient  $(\partial P_{MM}/\partial M)$ , where  $P_{MM}$  is the diagonal element of electron pressure) is possible even in a 2D, quasistatic model. Crescent-shaped distributions, however, are evident in this event (Li et al. 2021) suggesting that off-diagonal pressure may be active (e.g., Hesse et al. 1999).

The idea of a preferred X-line direction has been discussed by Genestreti et al. (2022) and small-angle deviations are seen in numerical simulations (Hesse et al. 2013; Daughton et al. 2011). To our knowledge, however, many kinetic simulations may not accept a nonorthogonal X-line due to a 2D system or boundary conditions that force an orthogonal X-line. These MMS observations therefore open up many questions that may require updated kinetic simulations and revisiting theoretical approaches to accept a nonorthogonal X-line.

This work was funded by the NASA MMS project (NNG04EB99C). J.E.S is supported by the Royal Society University Research Fellowship URF\R1\201286. The MMS spacecraft data used in Letter are available at https://lasp.colorado.edu/mms/sdc/public/links/.

#### ORCID iDs

Neha Pathak https://orcid.org/0000-0001-5567-8183
R. E. Ergun https://orcid.org/0000-0002-3096-8579
Y. Qi https://orcid.org/0000-0002-0959-3450
T. Vo https://orcid.org/0000-0002-8335-1441
M. E. Usanova https://orcid.org/0000-0002-0406-6387
T. D. Phan https://orcid.org/0000-0002-6924-9408
J. F. Drake https://orcid.org/0000-0002-9150-1841
S. Eriksson https://orcid.org/0000-0002-5619-1577
A. Chasapis https://orcid.org/0000-0001-8478-5797
J. E. Stawarz https://orcid.org/0000-0002-5702-5802
J. L. Burch https://orcid.org/0000-0003-0452-8403
R. B. Torbert https://orcid.org/0000-0001-7188-8690
R. Nakamura https://orcid.org/0000-0002-2620-9211

### References

```
Burch, J. L., & Drake, J. F. 2009, AmSci, 97, 392
Burch, J. L., Moore, T. E., Torbert, R. B., & Giles, B. L. 2015, SSRv, 199, 5
Burch, J. L., Torbert, R. B., Phan, T. D., et al. 2016, Sci, 352, aaf2939
Daughton, W., Roytershteyn, V., Karimabadi, H., et al. 2011, NatPh, 7, 539
Denton, R. E., Sonnerup, B. U. O., Russell, C. T., et al. 2018, JGRA, 123, 2274
Drake, J. F., Swisdak, M., Cattell, C., et al. 2003, Sci, 299, 873
Dunlop, M. W., Southwood, D. J., Glassmeier, K.-H., & Neubauer, F. M.
   1988, AdSpR, 8, 273
Eastwood, J. P., Phan, T. D., Bale, S. D., & Tjulin, A. 2009, PhRvL, 102,
Ergun, R. E., Ahmadi, N., Kromyda, L., et al. 2020a, ApJ, 898, 153
Ergun, R. E., Ahmadi, N., Kromyda, L., et al. 2020b, ApJ, 898, 154
Ergun, R. E., Tucker, S., Westfall, J., et al. 2016, SSRv, 199, 167
Forbes, T. G., & Priest, E. R. 1987, RvGeo, 25, 1583
Genestreti, K. J., Li, X., Liu, Y.-H., et al. 2022, PhPl, 29, 082107
Genestreti, K. J., Varsani, A., Burch, J. L., et al. 2018, JGRA, 123, 1806
Hesse, M., Schindler, K., Birn, J., & Kuznetsova, M. 1999, PhPl, 6, 1781
Hesse, M., Neukirch, T., Schindler, K., Kuznetsova, M., & Zenitani, S. 2011,
   SSRv, 160, 3
```

```
Hesse, M., Aunai, N., Zenitani, S., Kuznetsova, M., & Birn, J. 2013, PhPl, 20,
  061210
Huang, Y.-M., & Bhattacharjee, A. 2016, ApJ, 818, 20
Karimabadi, H., Roytershteyn, V., Daughton, W., & Liu, Y.-H. 2013, SSRv,
Lapenta, G., Krauss-Varban, D., Karimabadi, H., et al. 2006, GeoRL, 33,
   10102
Lazarian, A., Eyink, G. L., Vishniac, E. T., & Kowal, G. 2015, Magnetic Fields
  in Diffuse Media, Vol. 407 (Berlin: Springer)
Laitinen, T. V., Pulkkinen, T. I., Palmroth, M., Janhunen, P., &
  Koskinen, H. E. J. 2005, AnGeo, 23, 3753
Li, W.-Y., Khotyaintsev, Y. V., Tang, B.-B., et al. 2021, GeoRL, 48,
  e2021GL093164
Lindqvist, P.-A., Olsson, G., Torbert, R. B., et al. 2016, SSRv, 199, 137
Liu, Y. H., Hesse, M., Li, T. C., Kuznetsova, M., & Le, A. 2018, JGRA,
   123, 4908
Mozer, F. S., Bale, S. D., & Phan, T. D. 2002, PhRvL, 89, 015002
Murphy, N. A., Sovinec, C. R., & Cassak, P. A. 2010, JGR, 115, A09206
Øieroset, M., Phan, T. D., Fujimoto, M., Lin, R. P., & Lepping, R. P. 2001,
   Natur, 412, 414
Paschmann, G. 2008, GeoRL, 35, L19109
Paschmann, G., Øieroset, M., & Phan, T. 2013, SSRv, 178, 385
Petschek, H. E. 1964, in The Physics of Solar Flares, AAS-NASA Symposium,
  (NASA SP-50), ed. W. H. Hess (Greenbelt, MD: NASA), 425
Priest, E. R., & Schrijver, C. J. 1999, SoPh, 190, 1
Phan, T. D., Eastwood, J. P., Shay, M. A., et al. 2018, Natur, 557, 202
Pollock, C., Moore, T., Jacques, A., et al. 2016, SSRv, 199, 331
Roytershteyn, V., Daughton, W., Karimabadi, H., & Mozer, F. S. 2012,
  PhRvL, 108, 185001
Russell, C. T., Anderson, B. J., Baumjohann, W., et al. 2016, SSRv, 199, 189
Shi, Q. Q., Tian, A. M., Bai, S. C., et al. 2019, SSRv, 215, 35
Sundkvist, D., Retinò, A., Vaivads, A., & Bale, S. D. 2007, PhRvL, 99, 025004
Torbert, R. B., Burch, J. L., Phan, T. D., et al. 2018, Sci, 362, 1391
Torbert, R. B., Russell, C. T., Magnes, W., et al. 2016, SSRv, 199, 105
Uzdensky, D. A. 2011, SSRv, 160, 45
Wilder, F. D., Ergun, R. E., Goodrich, K. A., et al. 2016, GeoRL, 43, 5909
Yamada, M., Kulsrud, R., & Ji, H. 2010, RvMP, 82, 603
```

Zweibel, E. G., & Yamada, M. 2009, ARA&A, 47, 291